www.amlett.com, www.vbripress.com/aml, DOI: 10.5185/amlett.2016.6135 Published online by the VBRI Press in 2016

Effect of the granulation of starting powder on superplastic deformation of hydroxyapatite

Ryo Yamazaki[1], Koji Morita[2], Yoshio Sakka[2] and Kiyoshi Itatani[1]*

[1]*Department of Materials and Life Sciences, Sophia University, 7-1 Kioi-cho, Chiyoda-ku, Tokyo 1028554, Japan*
[2]*Advanced Key Technologies Division, National Institute for Materials Science, 1-2-1 Sengen, Tsukuba, Ibaraki 3050047, Japan*

*Corresponding author. Tel: (+81) 33238-3377; E-mail: itatani@sophia.ac.jp

Received: 02 September 2015, Revised: 17 November 2015 and Accepted: 23 December 2015

ABSTRACT

The effect of the granulation of starting powder on the superplasticity of hydroxyapatite ($Ca_{10}(PO_4)_6(OH)_2$, HAp) specimen was examined; the tensile elongation of specimen at high temperature was measured in order to evaluate the superplastic deformation. The translucent ceramics were fabricated using HAp powders with and without granulate (HAp and *g*-HAp) through the pulse current pressure sintering at 1000 ºC for 10 min: the mean grain sizes in both cases were approximately 0.2 μm. The tensile elongation of *g*-HAp specimen at 1000 ºC was 289 % (strain rate: 1.2×10^{-3} s^{-1}). The tensile stress was always lower than 30 MPa with maximum stress of 28.3 MPa, in contrast to the case of HAp specimen showing the maximum stress of 75.3 MPa (tensile elongation: 344 %). The lower stress of *g*-HAp specimen, compared to the case of HAp specimen, indicated the weak bonding of grains, but the failure being occurred by the concentrated stress at the strong bonding sites.

Keywords: Hydroxyapatite; superplasticity; pulse current pressure sintering.

Introduction

The hydroxyapatite ($Ca_{10}(PO_4)_6(OH)_2$, HAp) is a chief component of the bones. Thus HAp ceramic devices are currently used to fill in the defect parts or space of bones. In these cases, the mechanical processing may be needed in order to match the sizes and shapes of the devices with the space of bones. However, the ceramics are generally brittle, and may be difficult to perform the elongation, compression and bending processes which are usually conducted for metals. Thus the novel technique is needed in order to mechanically process the ceramics.

A superplasticity is defined as the ability to exhibit tensile elongation that is generally higher than 100 %. The ceramics to achieve such superplasticity must be: (i) high-density, (ii) sub-micrometer scaled grain sizes and (iii) weak bonding of grains, thereby accelerating the grain-boundary sliding. Owing to such grain-boundary sliding, the notable deformation occurs when the tensile or compressive force is applied to the ceramics at high temperature [**1**]. The superplasticity of HAp specimen was examined by Wakai *et al*. [**2**], who reported that the HAp specimen with the mean grain size of 0.64 μm was fabricated by the hot isostatic pressing at 1050 ºC for 2 h under the argon pressure of 203 MPa, and that the tensile elongation at 1050 ºC attained 153 % at the strain rate of 1.44×10^{-4} s^{-1}. The present authors fabricated HAp specimen with a relative density of 99.2 % and mean grain size of 0.56 μm by pressureless firing at 1100 ºC for 5 h, and investigated the superplastic deformation; the tensile elongation at 1100 ºC was 157 % at the strain rate of 1.5×10^{-4} s^{-1} [**3**]. Further, Yoshida *et al*. [**4**] reported that HAp specimen with mean grain size of 0.17 μm was fabricated by the pulse-current pressure sintering (PCPS) at 1000 ºC for 10 min under the pressure of 80 MPa; the tensile strain of HAp specimen achieved 486 % at the strain rate of 1.0×10^{-4} s^{-1}. As these researches indicate, the notable superplastic elongation is achieved when the sintering conditions and tensile test conditions match well with those for superplastic deformation.

The fabrication of high density HAp ceramics with sub-micrometer scaled grains for the realization of superplasticity required not only strictly-controlled sintering techniques but also utilization of high-quality starting powder. Regarding the high-quality HAp powder, HAp granules with the nanometer-scaled particles have started to be available from the manufacture, as well as non-granulated HAp powder with nanometer-scaled HAp particles. During the forming operation of the granulated powder, such granules are broken into individual particles, and these particles must be homogeneously rearranged toward closer packing, compared to the case of non-granulated powder. Nevertheless, little information regarding the effect of such granules on the superplasticity of dense HAp specimen, as well as the densification behavior, has been available until now.

On the basis of such background, the present paper describes the effect of granulation of starting particles on the densification of HAp ceramics and evaluation of the superplasticity.

Experimental

Fabrication of HAp ceramics

The starting HAp powders (HAP-100 (HAp) and granulated HAP (*g*-HAp)) were provided by Taihei Chem. Ind. Co., Ltd., Osaka, Japan. Two kinds of powder compacts were fabricated in this research. A cylindrical compact with a diameter of 20 mm and a thickness of approximately 3 mm was fabricated by uniaxially pressing approximately 1.5 g of the powder at 50 MPa, followed by pressureless firing. On the other hand, a cylindrical compact with a diameter of 30 mm and a thickness of approximately 3 mm was fabricated by uniaxially pressing approximately 10 g of the powder at 50 MPa, followed by a pulse-current pressure sintering (PCPS; SPS-1050, Sumitomo Coal Mining Co., Tokyo) at 1000 ºC for 10 min under a pressure of 50 MPa; the heating rate from room temperature to the desired temperature was fixed at 25 ºC min^{-1}.

Evaluation

Phase identification was conducted using an X-ray diffractometer (XRD: RINT 2000 V/P, Rigaku Corp., Tokyo, 40 kV and 40 mA) with monochromatic CuKα radiation, and using a Fourier transform infrared spectroscopy (FT-IR; 8600PC, Simadzu Corp., Kyoto).The compressive strength of each granule was measured using a microcompression tester (MCT-211; Shimadzu, Tokyo). The expansion-shrinkage of powder compact was examined using a thermo-mechanical analyzer (TMA; Model TAS-100, Rigaku, Tokyo) at a heating rate of 10 ºC·min^{-1}; a cylindrical specimen with a diameter of 5 mm and a thickness of 3 mm was fabricated by uniaxially pressing approximately 0.1 g of the powder at 50 MPa. The relative density of the sintered body was calculated on the basis of bulk density and theoretical density (= 3.16 gcm^{-3}); the bulk density was measured by the Archimedes method, using ethanol as a replacement liquid. The microstructure of sintered body was observed using a field-emission scanning electron microscope (FE-SEM; Model S-4500, Hitachi, Tokyo, Japan) with an accelerating voltage of 2 kV. On the basis of FE-SEM micrographs, the grain sizes were determined by multiplying π/2 by the linear intercept lengths. The microstructure of sintered body was observed using a high-resolution transmission electron microscope (HR-TEM; JEM-2100F, JEOL, Tokyo, Japan) with an accelerating voltage of 200 kV. The tensile test of the resulting specimens was conducted in air at a temperature of 1000 ºC under a strain rate of 1.2×10^{-3} s^{-1} and gauge length of 9 mm on a universal testing machine (TENSILON-1310, A&D Company, Tokyo, Japan) equipped with an infrared furnace. The tensile stress - strain relationship was obtained by assuming that uniform linear deformation occurred during the elongation.

Results and discussion

Properties of starting materials

Firstly, XRD pattern and FT-IR spectrum of *g*-HAp powder are shown in **Fig. 1**. XRD pattern of *g*-HAp powder, as well as the HAp powder (not shown here), included only the presence of HAp (JCPDS #09-0432). Moreover, FT-IR spectrum included the absorption peaks at 561, 602, 633, 1028, 1093 and 3692 cm^{-1}, and broad bands in the range of 1400 - 1600, 1700 - 1800 and 3200 - 3700 cm^{-1}.

Absorption peaks at 561 and 602 cm^{-1} are assigned to the bending vibration of P–O and P=O groups; the peaks at 1028 and 1093 cm^{-1} are assigned to the stretching vibration of P–O and P=O groups, whereas the peak at 633 and 3692 cm^{-1} is assigned to that of O–H group [**5**]. The broad bands in the ranges of 1700-1800 and 3200-3700 cm^{-1} are assigned to the stretching vibration of H–O–H group, which may be attributed to the presence of physically-adsorbed water. On the other hand, the broad band in the range of 1400 – 1600 cm^{-1} is assigned to the stretching vibration of carbonate ions (CO_3^{2-}) [**5**]. Thus the powder contains small amount of carbonate ions within HAp structure.

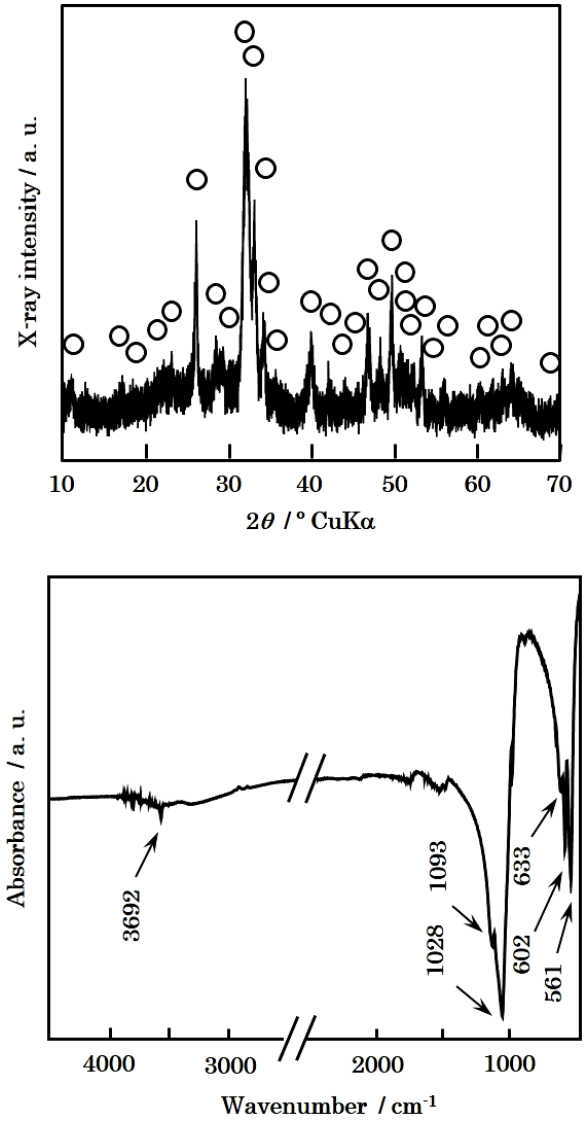

Fig. 1 XRD pattern (upper figure) and FT-IR spectrum (lower figure) of *g*-HAp powder.
(○: HAp)

The observation of starting HAp and *g*-HAp powder was conducted by using FE-SEM and HR-TEM. FE-SEM/HR-TEM micrographs and the particle size

distribution are shown in **Fig. 2**, together with the compressive strengths of granules. FE-SEM micrograph showed that the powder was composed of spherical granules with diameters of 1 to 100 μm (mean: 25.4 μm). It was found from the HR-TEM observation that the spherical granules were composed of rod-shaped particles with sizes of approximately 20 nm and that these rod-shaped particles contained pores (see arrow marks). Further, the compressive strengths of granules that were measured for 10 agglomerates were in range of 3 to 13 MPa with the mean value of 6.3 MPa.

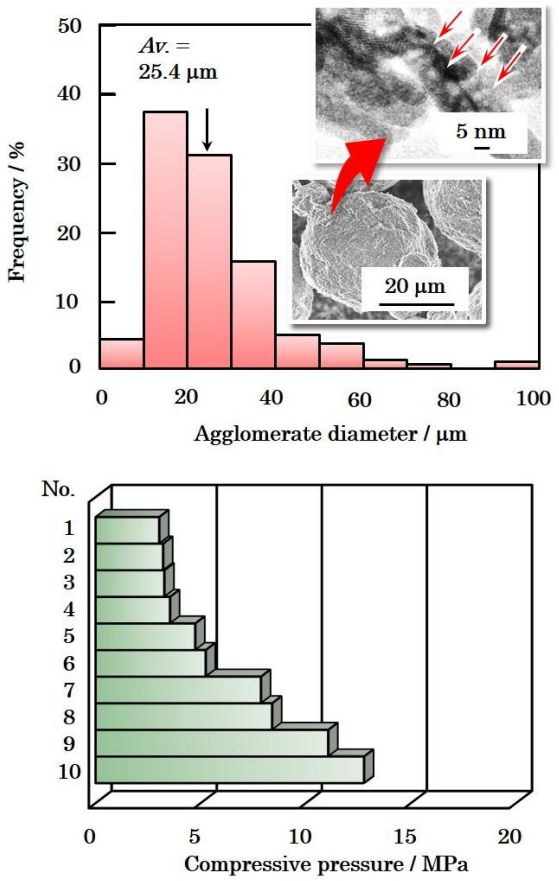

Fig. 2. FE-SEM and HR-TEM micrographs of *g*-HAp particles and particle size distribution (arrow marks in HR-TEM: pores within rod-shaped particles), and compressive strength of granules.

These granules seem to be broken into smaller particles below the pressures of 15 MPa. Thus these granules may be broken into particles to fill in the space within the compact when the forming pressure (50 MPa) is applied to this powder.

The individual particle size and shape of HAp powder are almost the same as those of *g*-HAp powder, considering that *g*-HAp powder seems to be prepared by the granulation of HAp powder.

Densification behavior during the pressureless firing

Prior to checking the relative densities of HAp ceramics, the densification behavior of the HAp compact was examined using TMA. The expansion-shrinkage curves of HAp compacts fabricated by using HAp and *g*-HAp powders (hereafter referred to as HAp and *g*-HAp compacts) are shown in **Fig. 3**, together with typical FE-SEM micrographs. The shrinkage of HAp compact started to occur at around 700 ºC; it was accelerated with a further increase in temperature, but was completed at around 1050 ºC. The differential curve showed that the shrinkage rate started to be accelerated at around 700 ºC, and that the maximum shrinkage rate was achieved at around 900 ºC. On the other hand, the shrinkage of *g*-HAp compact started to occur at approximately 750 ºC; it was accelerated with a further increase in temperature, but was completed at around 1100 ºC. The differential curve showed that the maximum shrinkage rate was achieved at around 950 ºC. FE-SEM micrograph of *g*-HAp compact heated up to 950 ºC showed that the grains with sizes of < 0.5 μm were closely packed, but that many pores were present on grain boundaries. FE-SEM micrograph of HAp compact heated up to 1100 ºC showed that the grains with mean grain size of 0.46 μm were closely packed, and that few pores were present on grain boundaries.

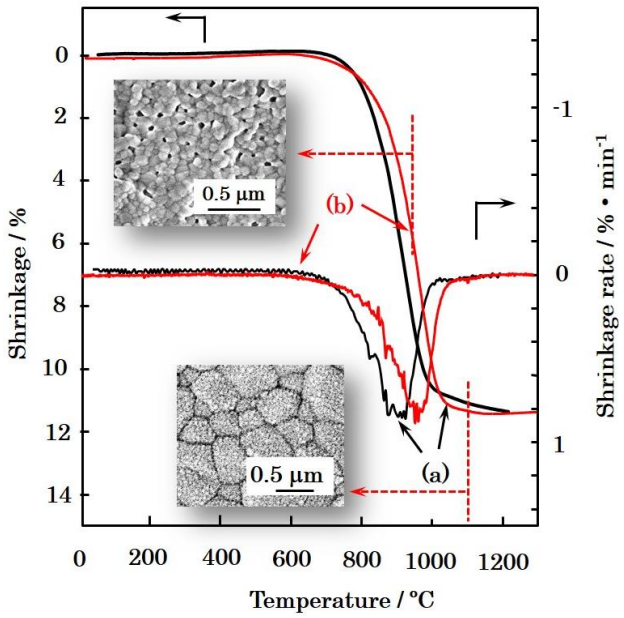

Fig. 3. Expansion-shrinkage curves and their differential curves of (a) HAp and (b) *g*-HAp compacts, together with typical SEM micrographs of *g*-HAp compacts heated up to 950 ºC and 1100 ºC.
Heating rate: 10 ºC·min^{-1}.

These results indicate that the densifications of HAp and *g*-HAp compacts are virtually completed at around 1100 ºC. Comparing the shrinkage behavior of *g*-HAp compact with that of HAp compact, the former shrinkage was a little retarded rather than the latter shrinkage. In order to make clear such difference in shrinkage behavior, HAp and *g*-HAp compacts were pressurelessly-fired at 1000 ºC, 1050 ºC and 1100 ºC for 5 h. The relative densities of *g*-HAp bodies fired at 1000 ºC to 1100 ºC for 5 h were in the range of 96.5 to 97.8 %. According to the FE-SEM observation, *g*-HAp body fired at 1000 ºC for 5 h was composed of closely-packed grains with sizes of 0.1 to 1.5 μm (mean grain size: 0.50 μm and 0.51 μm, respectively). The grain size of *g*-HAp body fired at 1100 ºC for 5 h were in range of 0.1 to 3 μm (mean grain

size: 0.76 μm). On the other hand, the relative density and grain size of HAp body fired at 1100 ºC for 5 h were 96.6 % and 0.59 μm, respectively. Comparing the relative density and grain size of *g*-HAp body with those of HAp body fired at 1100 ºC for 5 h, the former relative density was higher and grain size was larger, compared to the latter case. This fact demonstrates that the gradual densification may be effective for the elimination of pores within the HAp body, but the densification encourages the grain growth, due to the increased contact areas of grains.

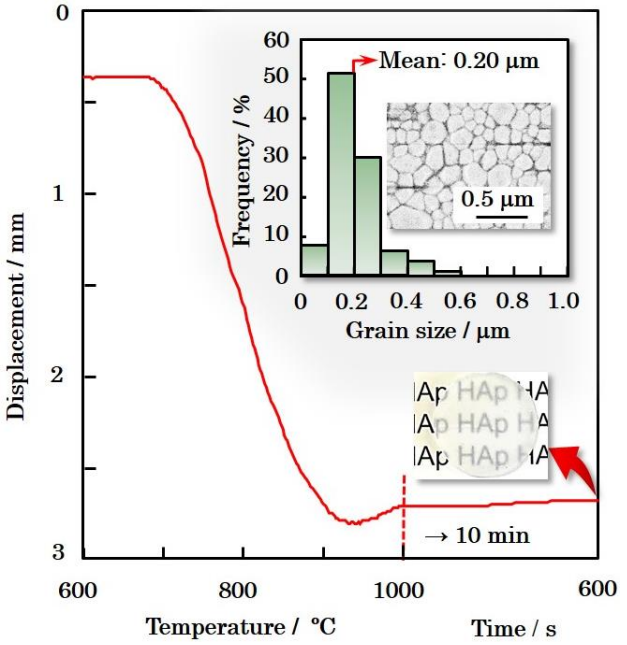

Fig. 4 Shrinkage-expansion curve of HAp compact during the PCPS, appearance of sintered HAp body, SEM micrograph and grain size distribution. Heating rate: 25ºC·min^{-1}.

Densification behavior during the PCPS

In order to fabricate more dense and fine grained HAp ceramics, PCPS was conducted at 1000 ºC for 10 min under the pressure of 50 MPa. In this research, the heating rate of 25 ºC min^{-1} was selected for the rapid densification and narrow grain size distribution, compared to the case of dilatometry investigation (10 ºC min^{-1}; see **Fig. 3**), both of which must be effective for the superplastic deformation, due to the smooth grain boundary sliding. The shrinkage curve with temperature/time is shown in **Fig. 4**, together with the translucent appearance and microstructure (FE-SEM micrograph) of resulting HAp body and grain size distribution. The shrinkage of the HAp compact started to occur at around 700 ºC, and increased with temperature; the densification was almost completed at around 950 ºC. After the temperature attained 1000 ºC, the expansion was observed during the firing at 1000 ºC. The resulting HAp body fabricated by PCPS at 1000 ºC for 10 min under the pressure of 50 MPa was translucent, and the relative density and mean grain size of the sintered HAp body were 99.5 % and 0.20 μm, respectively. The grain sizes were in range of 0 to 0.6 μm. XRD pattern showed that the sintered HAp body was composed of only HAp (data not shown here).

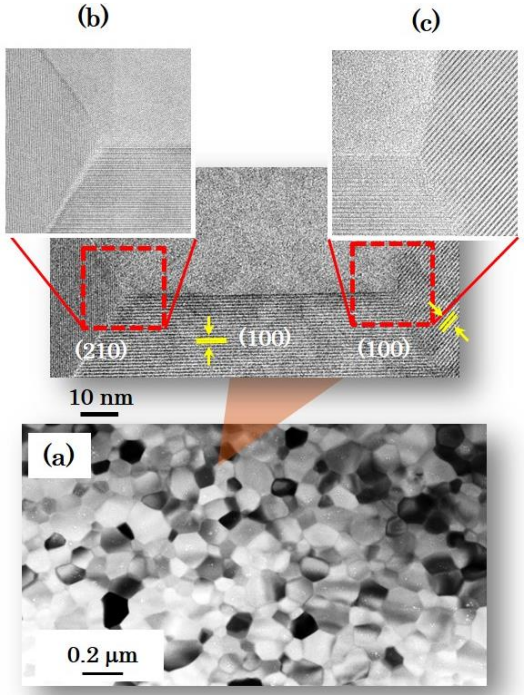

Fig. 5. HR-TEM micrograph of HAp body fabricated by PCPS at 1000ºC for 10 min.

Fig. 5 shows the HR-TEM micrographs showing the microstructure and the lattice fringes. The microstructure showed that the grains with sizes of 0.2 □m were closely packed one another (**Fig. 5(a)**). The lattice fringes had inter-planar spacing consistent with (100) and (210) planes of the HAp structure; the lattice disorder was observed at the interfaces where these atomic planes were in contact with one another (**Fig. 5(b)**). The lattice fringes of other sides showed that the planes were closely contact with one another (**Fig. 5(c)**). A portion of interface of adjacent grains shows the lattice disorder, together with the interface with the joining of lattice. These characteristic sites are thus found to be included at the interface of grains.

High temperature tensile test

Since high density and fine-grained HAp and *g*-HAp body could be fabricated by PCPS, the tensile elongation of these specimens was conducted at the test temperature of 1000 ºC with the results being shown in **Fig. 6**, together with the grain deformation. The stress of HAp specimen increased with strain and showed maximum (75 MPa), followed by the failure at the strain of 344 % (**Fig. 6(a)**). The stress of *g*-HAp specimen increased to a maximum value with increasing strain, followed by the failure at 289 %; the stress was in range of 15-30 MPa during the tensile test. Compared to the stress-strain curve of *g*-HAp specimen with that of HAp specimen, the former stress was always below 30 MPa, in contrast the case of HAp specimen (approximately 75 MPa). This fact indicates that *g*-HAp specimen has potentials to show the notable elongation being comparable to or more than the case of HAp specimen. A grain deformation appeared to be occurred by the notable tensile elongation of specimen. Simultaneously, the cavity was created within the elongated specimen (see FE-SEM micrograph in **Fig. 6(b')**).

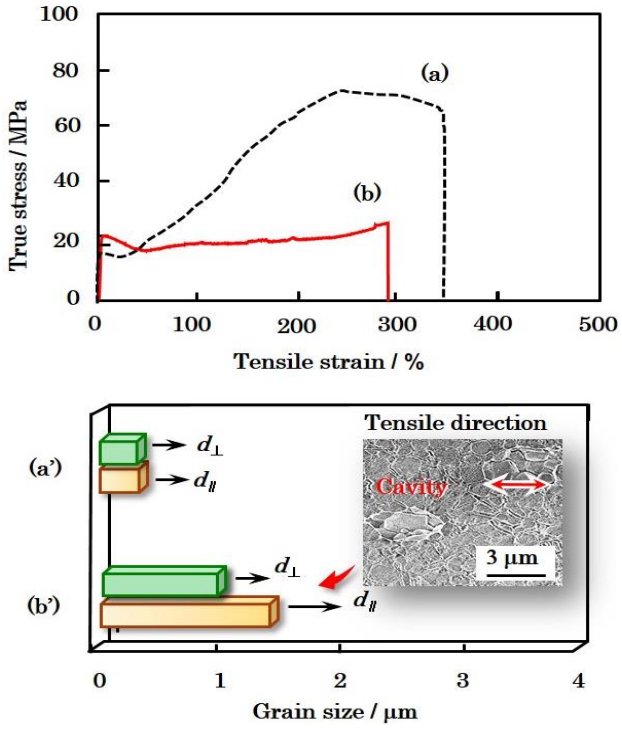

Fig. 6. Stress-strain curves of (a) HAp specimen [**6**] and (b) *g*-HAp specimen at the strain rate of 1.2 x 10^{-3} s^{-1}(upper figure), and the grain sizes parallel and perpendicular to the tensile direction of HAp specimen (a') before and (b') after the tensile test (lower figure), together with FE-SEM micrograph.

The average $d_{//}$ (grain size parallel to the tensile direction) and $d_{\perp}$ (grain size perpendicular to the tensile direction) were 1.29 μm and 0.89 μm, respectively; the ratio of $d_{//}$ to $d_{\perp}$ was therefore 1.45.The total strain may be calculated on the basis of these values. Assuming that a cubic-shaped grain is deformed, the apparent inter-granular strain, ε_g, is given by [**2**]:

$$\varepsilon_g = (2/3) \ln (d_{//}/d_{\perp}) \quad (1)$$

From Eq. (1), the value of ε_g is 0.248. The total strain, ε_T, is expressed as follows:

$$\varepsilon_T = \ln ((L_0 + l) / L_0) \quad (2)$$

where, L_0 is an original gauge length and l is an elongation to the failure. Based upon Eqs. (1) and (2), the contribution of grain boundary sliding to the total strain, A, may be defined as follows [**2**]:

$$A = 100 (1 - (\varepsilon_g / \varepsilon_T)) \quad (3)$$

The value of A of *g*-HAp specimen, for example, is estimated to be 81.8 %. Thus the grain-boundary sliding seems to be predominantly occurred during the deformation. Such difference in tensile strain and stress between *g*-HAp and HAp specimens may be attributed to the difference in efficiency of grain-boundary sliding.

The schematic diagram of the slow and rapid grain boundary sliding is illustrated in **Fig. 7**. When the elongation is notably progressed with strain, no marked stress may be concentrated on and near the grain boundaries, due to the efficient sliding of grains. In contrast, when the elongation is restricted, regardless of the increase in strain, the stress may be concentrated on and near the grain boundaries, thereby leading to the failure. The grain-boundary sliding must be accelerated with decreasing bonding strength among grains, *e.g.*, the misorientation of crystalline lattice (lattice disorder) and/or the presence of amorphous phase on grain boundaries.

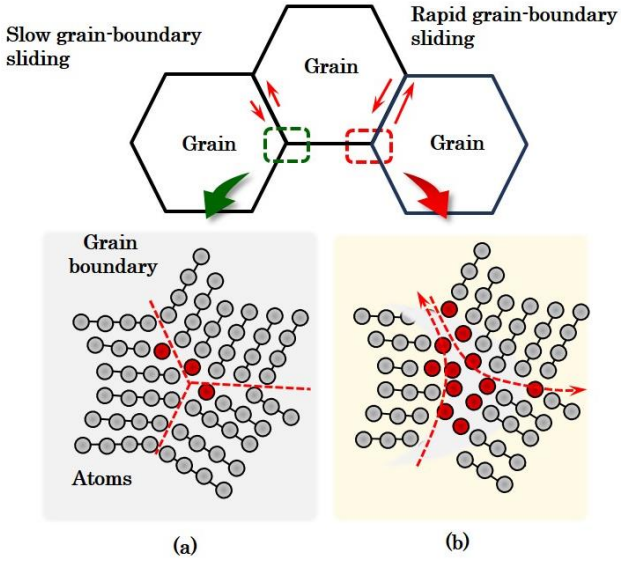

Fig. 7. Schematic diagram of slow and rapid grain boundary sliding among grains.
(a) Slow grain boundary sliding
(b) Rapid grain boundary sliding
Note that the slow grain boundary sliding causes higher tensile strain, while the rapid grain boundary sliding causes the lower tensile strain.

During the tensile elongation, *g*-HAp specimen showed significantly lower tensile stress than that of HAp specimen. For example, the tensile stress being approximately 70 - 75 MPa for 118 to 455 % elongations [**2 - 4**]. This fact indicates that *g*-HAp specimen may be deformed more easily, compared to the case of HAp specimen, because the lower stress encourages the smooth grain-boundary sliding. Thus *g*-HAp specimen has potentials to show the notable elongation being comparable to or more than the case of HAp specimen.

Overall, we have the possibility to fabricate the dense HAp specimen without the PCPS apparatus, owing to the utilization of granulated powder. We will check the biological performance of resulting HAp specimen and report the results elsewhere.

Conclusion

We investigated the superplastic deformation of high density and fine grained HAp and *g*-HAp bodies fabricated using PCPS. The results obtained in this study were summarized as follows:

(1) The translucent HAp and *g*-HAp ceramic bodies with grain size of 0.2 mm could be fabricated by PCPS at 1000 ºC for 10 min under the pressure of 50 MPa.

(2) The tensile elongation of *g*-HAp specimen was examined at the test temperature of 1000 ºC and strain rate of 1.2×10^{-3} s^{-1}. The tensile elongation of *g*-HAp specimen was 289 %, and the tensile stress during the tensile test was always smaller than 30 MPa with maximum stress of 28.3 MPa. This maximum stress was about 47 MPa, being lower than that of the HAp specimen (75.3 MPa).

Acknowledgements

The authors expressed their thanks to Dr. Takeshi Toyama (Nihon Univ.) for the measurement of compressive strength of granules.

Reference

1. Wakai, F.; *J. Ceram. Soc. Japan*, **2004**, *112*, 472. **DOI:** 10.2109/jcersj.112.472
2. Wakai, F.; Kodama, Y.; Sakaguchi, S.; *J. Am. Ceram. Soc.*, **1990**, *73*, 457. **DOI:** 10.1111/j.1151-2916.1990.tb06537.x
3. Tago, K,; Itatani, K.; Suzuki, S. T.; Sakka, Y.; Koda, S.; *J. Ceram. Soc. Japan*, **2005**, *113*, 669. **DOI:** 10.2109/jcersj.113.669
4. Yoshida, H.; Kim, B-N.; Son, H-W.; Han, Y-H.; Kim, S.; *Scr. Mater.*, **2013**, *69*, 155. **DOI:** 10.1016/j.scriptamat.2013.02.044
5. Koutsopoulos, S.; *J. Bio. Mater. Res.*, **2002**, *62*, 600. **DOI:** 10.1002/jbm.10280
6. Itatani, K.; Tsuchiya, K.; Sakka, Y.; Davis, I. J.; Koda, S.; *IOP Conf. Ser. Mater. Sci. Eng.*., **2011**, *18*, 022020 **DOI:** 10.1088/1757-899X/18/2/022020

